Everlast: Long-life, Supercapacitor-operated Wireless Sensor Node

Farhan Simjee and Pai H. Chou
Center for Embedded Computer Systems, University of California, Irvine, CA 92697-2625 USA
Email: {fsimjee,phchou}@uci.edu

ABSTRACT

This paper describes a supercapacitor-operated, solar-powered wireless sensor node called Everlast. Unlike traditional wireless sensors that store energy in batteries, Everlast's use of supercapacitors enables the system to operate for an estimated lifetime of 20 years without any maintenance. The novelty of this system lies in the feedforward, PFM (pulse frequency modulated) converter and open-circuit solar voltage method for maximum power point tracking, enabling the solar cell to efficiently charge the supercapacitor and power the node. Experimental results show that Everlast can achieve low power consumption, long operational lifetime, and high transmission rates, something that traditional sensor nodes cannot achieve simultaneously and must trade-off.

Categories and Subject Descriptors

C.3 [**Special-Purpose and Application-Based Systems**]: Real-time and embedded systems

General Terms

Management, Measurement, Performance, Design

Keywords

Maximum power point tracking, supercapacitor, solar power, wireless sensors

1. INTRODUCTION

Wireless sensor nodes are being deployed for new applications that are demanding higher data rates in large-scale networks with up to thousands of nodes. Today, many wireless sensor nodes achieve low power by low duty cycling. Going to higher data rates will dictate the use of high-capacity batteries and possibly solar cells to replenish the energy regularly. At the same time, large-scale deployment will demand lower cost per node.

Among the ultra low-power, low-cost radios with 1kbps data rate and a range of 3–10 meters, PicaRadio may run for several years without battery recharging or replacement [1, 2]. While useful for some applications, in order to achieve a 10–20 year operational lifetime, these nodes must operate at much lower duty cycles than one transmission per minute. The widely used Mica2 mote [3] uses a 38.4 kbps radio with a range of $>$80 meters in ground-level, line-of-sight communication. Powered by two AA batteries, it can run for a few hours in 100% duty cycle, or a few months when activated by a threshold detector with very infrequent events. With some external circuitry and a solar panel, the batteries can be recharged each day for significantly extended operations [4]. Due to the limited number of recharge cycles, the battery will require replacement after one to two years. Unfortunately, such recurring maintenance cost is likely to become very expensive or prohibitive if it must be done for thousands of deeply embedded nodes, which are likely to be difficult or expensive to access after deployment.

In both cases above, the battery is the primary limiting factor that prevents the node from operating maintenance-free for more than several years at non-trivial data rates. One solution that slows down battery aging is to place a supercapacitor in parallel with the battery so that transient power is delivered by the capacitor rather than the battery [5, 6, 7]. Fewer and shorter current pulses drawn from the battery allow more efficient use of battery capacity and increase the number of charge cycles possible. Also, a supercapacitor has been used to buffer solar energy for a few days to weeks to reduce the need for daily battery charging [8]. Unfortunately, even with less-frequent recharges the battery is still limited to holding charge for a few years before a reduction in energy capacity.

By removing the battery altogether and storing energy solely in the supercapacitor, there is now a viable option for achieving long-life operation. Supercapacitors have received wide attention recently due to their power density, low equivalent series resistance (ESR), and very low leakage current [9]. A typical supercapacitor offers more than half a million charge cycles and a 10-year operational lifetime until the capacity is reduced by 20%. At this point 80% of the useful energy is still available because the ESR is still very low unlike a battery whose useful energy drops to 50% at this point because the higher ESR causes premature end of life. By designing the node to operate on 50% energy capacity, the operational lifetime can be pushed out to 20 years.

The energy density of supercapacitors today is still less than batteries by an order of magnitude. However, when used in conjunction with a suitable solar cell, the supercapacitor should be able to sufficiently power the node when there is not enough sunlight in the environment. Aggressive power management techniques should also be able to close the energy density gap between supercapacitors and batteries. Given that a 350F capacitor with a capacity of 240 mAh from Maxwell Technologies costs $20 in single quantity, supercapacitors are also becoming competitive with rechargeable Li-ion batteries. Since a single supercapacitor will outlive half

ISLPED'06, October 4–6, 2006, Tegernsee, Germany.

a dozen batteries, the drastically reduced maintenance costs and the anticipated price drop with volume are expected to significantly lower the overall cost of operating the sensor network.

The purpose of this work is to demonstrate the feasibility of such a sensor node operating on supercapacitors recharged by solar cells. One could not simply replace a battery with a supercapacitor because of the very different electrical characteristics and efficiency considerations in relation to the solar cells. We propose a feed-forward, pulse frequency modulated regulator that charges the supercapacitor at the optimal operating point for solar cells. We have constructed a complete wireless sensor node called Everlast with this solar/supercapacitor power circuitry and stress-tested its operation. Experimental results show that the Everlast node can achieve low power consumption, long operational lifetime, and high transmission rates simultaneously, without forcing the user to make trade-offs. This is expected to enable a whole new class of applications for low-cost, high performance, durable wireless sensor networks.

2. RELATED WORK

Charging a capacitor and drawing maximum solar power are both areas of active research. However, the authors are not aware of prior work on efficiently charging a capacitor using optimal solar power. The problem with capacitor charging is that a when large capacitor is attached to a solar cell, the component acts as a short and the solar voltage drops to the capacitor voltage. Although the solar cell will charge under this condition, it will not do so efficiently, because it will not be at the *maximum power point* (MPP), the voltage and current combination that maximizes power output under a given sunlight and temperature condition. A supercapacitor has been charged in this manner before but this reduces the solar efficiency by a factor of 2-5x depending on the solar cell topology [8].

A typical PWM regulator is not suitable because the ESR in the supercapacitor is so low that only a short pulse will prevent the supply voltage to fall sharply. For this reason, pulse power applications use resonant and Ward converters to efficiently and quickly charge capacitors [10, 11]. Unfortunately, the resonant converter requires an AC voltage that cannot be generated by the solar panel. The Ward converter inputs DC power, but the circuit is rather complex and requires a low impedance power source such as a battery or electrical outlet. Clearly, a new converter design is needed to meet the requirement of efficiently charging a capacitor from a high impedance power source.

The MPP also changes for a solar cell across temperature and sunlight. Numerous methods proposed to date for tracking the solar cell MPP include the hill climbing method, short-circuit method, and open-circuit voltage method [12, 13, 14, 15]. The hill climbing method of sweeping solar voltage while measuring the current requires a great deal of circuitry in the form of a microcontroller (MCU) to calulate the optimal power point. The power needed to run those chips are too high to keep the converter efficient. The short circuit method entails shorting the solar cell and measuring the short circuit current, which directly determines the MPP [16]. Finally, the open-circuit voltage method simply requires disconnecting the solar cell from any load and measuring the open-circuit solar voltage, which again is directly related to the MPP [17, 18]. The latter two methods are not as accurate as the hill climbing method, but are easy to implement with low power overhead.

3. PROBLEM STATEMENT

The problem is to build a power converter that can efficiently charge a large capacitor at the optimal voltage and current of the solar cell. Since the goals are cost reduction and circuit simplicity, the solution will require trade-offs among the efficiency of the power converter, cost, and the accuracy of the maximum power point tracking (MPPT) circuitry, and power overhead.

The regulator control circuitry must be able to both set the voltage or current to the optimal value and make corrections when the solar cell deviates from this value. Unlike a typical voltage regulator that uses feedback from the output, our converter requires the solar cell input to be fed forward into the control circuitry. To formulate the MPP problem, we define the following variables:

E : plane-of-array solar irradiance (W/m^2)
E_e : effective irradiance, or "suns"
AM_a : absolute air mass (dimensionless)
AOI : solar angle-of-incidence on module (degrees)
T_c, T_o : temperature of cells and reference temperature (Celsius)
I_{sco}, I_{mpo} : ref. short-circuit current and ref. max. power current
V_{oco}, V_{mpo} : ref. open-circuit voltage and ref. max. power voltage
$\alpha_{I_{sc}}, \alpha_{I_{mp}}$,
$\beta_{V_{oc}}, \beta_{V_{mp}}$: temperature coefficients
$C_0 - C_4$: empirical coefficients
$K_{I_{mp}}, K_{V_{mp}}$: constants to calculate I_{mp} and V_{mp} from I_{sc} and V_{oc}

$$I_{sc}(E, T_c, AM_a, AOI) = (E/E_o) f_1(AM_a) f_2(AOI) \cdot (I_{sco} + \alpha_{I_{sc}}(T_c - T_o)) \quad (1)$$

$$E_e = \frac{I_{sc}(E, T_c = T_o, AM_a, AOI)}{I_{sco}} \quad (2)$$

$$I_{mp}(E_e, T_c) = C_0 + E_e(C_1 + \alpha_{I_{mp}}(T_c - T_o)) \quad (3)$$

$$V_{oc}(E_e, T_c) = V_{oco} + C_2 \ln(E_e) + \beta_{V_{oc}}(T_c - T_o) \quad (4)$$

$$V_{mp}(E_e, T_c) = V_{mpo} + C_3 \ln(E_e) + C_4(\ln(E_e))^2 + \beta_{V_{mp}}(T_c - T_o) \quad (5)$$

$$\frac{\partial P_{solar}}{\partial V_{solar}} = \frac{\partial P_{solar}}{\partial I_{solar}} = 0 \quad (6)$$

$$V_{mp} = K_{V_{mp}} V_{oc} \quad (7)$$

$$I_{mp} = K_{I_{mp}} I_{sc} \quad (8)$$

The maximum power described in (3) and (5) is directly dependent upon the solar intensity and the temperature [19]. Under a given sunlight condition, (6) holds when the solar power output is maximized. Since it would be difficult to empirically find MPP at runtime without a PC and a correct solar model, finding the power peak will require the brute force hill-climbing technique and some computation. Fortunately, it also known that the voltage and current at MPP are directly proportional to V_{oc} and I_{sc}, as described by (7)(8), respectively [16, 17]. This method would simply require the regulator to shut down for a few moments to measure V_{oc} or I_{sc} to find the new MPP, and adjust the power converter. With these techniques, MPP can be reached more quickly since it requires only a single computation and a momentary shutdown of the converter.

4. EVERLAST SYSTEM DESIGN

Fig. 1 shows an overview of the Everlast design. The system is designed for three primary tasks: charging the capacitor using a pulse-frequency modulated (PFM) regulator, feeding the PFM controller the optimal operating point for the solar cell, and all the typ-

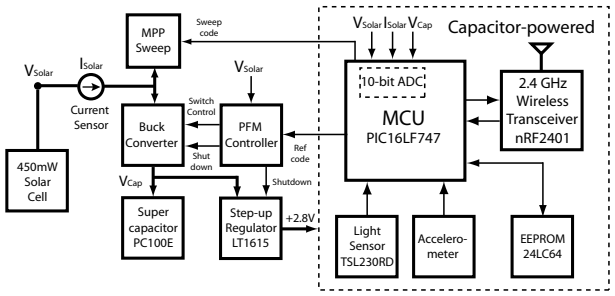

Figure 1: Everlast system block diagram

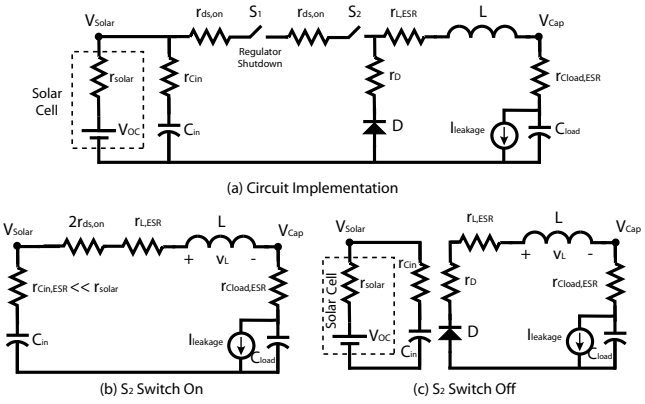

Figure 2: PFM Regulator

ical WSN functions including reading sensor data and communication with nodes and basestations through the wireless transceiver.

4.1 PFM Regulator

Since the capacitor is seen as a short to the solar cell when they are connected together, the traditional voltage regulators such as the PWM DC-DC converter and linear regulator would not function properly because V_{solar} would quickly fall to V_{cap} and greatly deviate from V_{mp}. With the feedback pin connected to the output load, the regulator would short the input and output until reaching the preset output voltage. As shown in Fig. 2, a PFM regulator is designed with the advantages of the switched-capacitor regulator and the buck converter to prevent shorting the input and output. At startup, the switch S_2 is open, and the solar cell charges the input capacitor. Once V_{solar} reaches the upper threshold of (9) which is set by the PFM Controller, S_2 is closed and C_{in} sends current to the inductor, L, and the supercapacitor, C_{load}. The current from the solar cell can be ignored in the on switch state, because the input capacitance ESR is much lower than the impedance of the solar cell. Since all these components have low resistive values, energy is transferred very quickly until the bottom threshold of (9) is met. Once switch S_2 is in the off state, C_{in} is once again recharged and the inductor transfers energy to C_{load} and thus charging the supercapacitor. Fig. 3 shows the solar voltage and pulses sent to the switch when the regulator is operating.

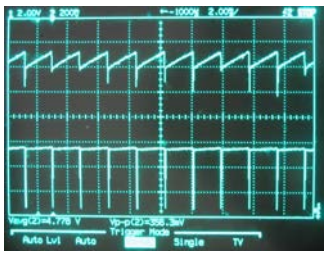

Figure 3: PFM Regulator Waveform: V_{solar} (top), S_2 (bottom)

The circuit is similar to a switched-capacitor circuit in that it charges a capacitor and then transfers that energy to the output load capacitor. The only difference is that an inductor is added to buffer the voltage difference between V_{solar} and V_{cap}. The pulse frequency is primarily dependent upon the switching thresholds, input capacitance, and solar power (Eqn. 10).

The regulator efficiency is measured with a test setup that is similar to a deployed sensor node but at the same time is easily reproducible. A solar cell is placed under a high-power adjustable halogen lamp so that it can produce constant power. The solar cell is fed to the PFM regulator to charge a 10F supercapacitor. The efficiency is calculated by charging the capacitor from 0V to 2.4V and 1V to 2.4V and comparing the total solar energy generated with the change in the energy stored in the capacitor (Eqn. 11).

Fig. 4 shows the results across varying solar power, and generally over 20mW the efficiency plateaus. Charging from 0V is less efficient, because the higher voltage difference V_{solar} and V_{cap} causes more parasitic losses. The efficiency curve with the capacitor already charged to 1V is a better indicator of real-world performance, as the sensor node is assumed to always be powered on.

C_{in} is also changed in the regulator to see how that affects operation. Since it is faster to charge a smaller capacitor, the frequency increases with smaller input capacitance. With 1μF C_{in}, the regulator can achieve 65% efficiency, because there is less resistive loss in the capacitor, MOSFET switch, and inductor at higher frequencies. As there is no sign of further efficiency loss due to dynamic power at higher frequencies, C_{in} can be further reduced. However, choosing an amplifier that modulates the switch with low supply current came at the cost of slower slew rate to drive the switch. If C_{in} is lowered, then the pulses will not fully turn on the FET. A future board revision will explore adding a FET gate driver and using power inductors, but as it stands, the regulator has been experimentally verified to operate in the 0.5Hz to 30kHz range across varying P_{solar} from 3mW to 300mW, respectively. No battery charger IC on the market can match this PFM regulator's ability to harvest low power. With a change of the passive components and switch, the regulator can also accommodate sub-mW piezoelectric generators and larger solar cells.

$$V_{mp} - V_{hyst} < V_{solar} < V_{mp} + V_{hyst} \tag{9}$$

$$f_{pulse} \propto \frac{1}{V_{hyst}} \frac{1}{C_{in}} \frac{1}{L} P_{solar}(t) \tag{10}$$

$$\eta = \frac{E_{solar}}{E_{cap,end} - E_{cap,start}} = \frac{P_{solar,avg} t_{chargetime}}{\frac{1}{2} C (V_{end}^2 - V_{start}^2)} \tag{11}$$

4.2 PFM Controller

The function of this PFM controller is to pulse the regulator every time V_{solar} exceeds the specified reference voltage, which is V_{mp} in this case. Fig. 5(a) shows V_{solar} being compared to a reference voltage to determine switching the regulator. Hysteresis is added to stabilize the amplifier and control the pulse frequency. The resistors are larger than the impedance coming from reference and solar cell so that V_{hyst} remains accurate (Eqn. 12,13). The voltage reference is divided by a cermet POT and an 8-bit digital POT,

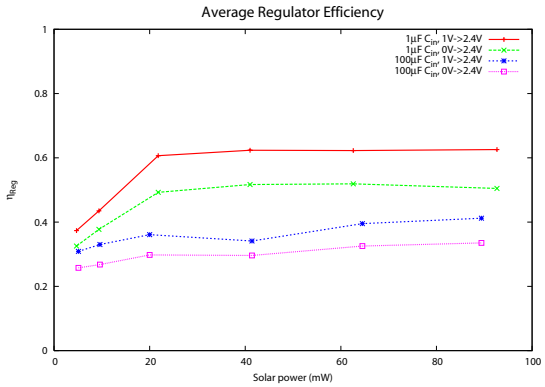

Figure 4: PFM Regulator Efficiency

and the solar voltage is resistively divided so that the amplifier can compare it with the reference signal. The digital POT defaults to 100kΩ and, along with the cermet POT, presets the solar voltage at which to regulate when the MCU is powered down.

The MCU fine-tunes the digital POT value until V_{solar} reaches V_{mp}. The MCU is used rather than some custom circuitry, because it is flexible enough to run any of the MPPT methods mentioned earlier. The hill climbing method can be achieved by sweeping the POT code while recording the voltage and current. The solar cell can be short-circuited momentarily by setting the POT value to 0 and thus closing the switch. Conversely, V_{oc} is measured by setting the POT value to 255 to open the switch. With the latter two, V_{mp} and I_{mp} can be easily calculated by the MCU using Eqns. (7)(8). With either of these values, the POT value can be adjusted until V_{solar} or I_{solar} reaches one of these respective values. Depending on whether an application requires accurate MPPT or low cost/complexity, the suitable method can be chosen and custom circuitry can be implemented.

As shown in Fig. 5(b), the functional block of the PFM controller also includes the ability to shut down the regulator when the capacitor is fully charged by comparing it with a 2.5V reference signal. The amplifier can be jumpered to also accept a signal from the MCU to shut down. In order to operate the sensor node from a dead start, the bootstrap circuitry in Fig. 5(c) keeps the step-up regulator shut down until V_{cap} reaches a high enough voltage that is set by voltage dividing from the 3.0V reference.

For testing purposes, the MPP sweep circuitry is included to sweep the circuit I_{solar} and measure V_{solar} to profile the solar cell as shown in Fig. 5(d). While the PFM regulator is shut down, the MCU sweeps the gate voltage of a MOSFET using a DAC. This sweeps the solar current, and both I_{solar} and V_{solar} are sampled after every DAC step. The MCU can then calculate P_{mp}, V_{mp}, and I_{mp} and take a light measurement to profile MPP at every light intensity level. The solar profile will be useful later to benchmark how accurately the MPPT methods can keep the solar cell at P_{mp}.

$$V_{hyst} = V_{ref}\frac{R_1}{R_1+R_2} \tag{12}$$

$$R_1, R_2 \gg R_3, R_4 \tag{13}$$

4.3 WSN Functions

Although the primary goal of Everlast is to keep the solar cells at MPP and operate for 20 years, some of the latest technologies in MCUs, sensors, and transceivers are adopted so that the board will

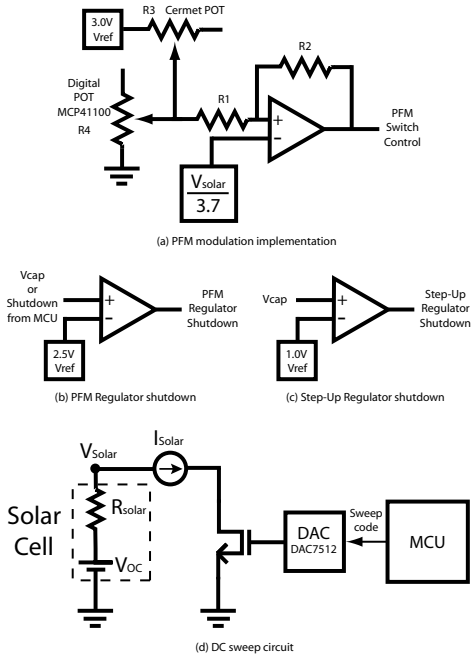

Figure 5: PFM Controller and DC sweep circuitry

operate with lower power requirements.

The PIC16LF747 is selected as the MCU because of its low supply current from 25μA at 31.25kHz to 930μA at 8MHz with V_{DD} at 3.0V using an internal RC oscillator. The MCU can operate from 2.0V to 5.5V and the internal RC oscillator can be controlled at runtime. There has been much work on dynamic voltage and frequency scaling (DVFS), and practically any of those techniques can be written into the firmware.

Most sensors today either produce an analog voltage, PWM signal, or PFM signal. The MCU can read the first using its internal 10-bit ADC or an external, possibly higher-precision, ADC. The latter two signals can be measured with an internal timer/counter or by polling. The TSL230RD light sensor improves upon traditional methods of measuring light intensity such as with a photodiode, because it has a pin-selectable light aperture for measuring a wider dynamic range of light. The light sensor draws 2mA when operating, but since it generates a square-wave output, the MCU can easily count the edges using the internal counter in a matter of 1–2 ms while consuming 12μJ per sampling. The ADXL202 is a dual-axis $\pm$ 2g accelerometer consuming 600μA. The supply current is low enough that the MCU I/O pin can power it during sampling and power it down otherwise. A few more ADC pins are drawn out to the board so that additional sensors can be added anytime. The board also includes an EEPROM that can be used for storing sensor data.

For wireless communication, we use the Nordic nRF2401 2.4GHz GFSK transceiver, a recent breakthrough in low power transceivers. Operating in the ISM band, it supports 125 channels and can support a dense network of sensor nodes. With the ability to send ShockBurst messages, the transceiver turns on to send a 256-bit packet in a 1Mbps datastream and goes back to standby. With 0dBm RF power, the transceiver has line of sight range of 300m according to the datasheet, and we have physically verified it for at least a 150m range. With integrated pseudo-MAC layer, the transceiver incorporates a 16-bit CRC and the destination address

Profile	MCU Core Freq. (MHz)	ADC Sampl./msg	Transceiver Msg/sec	I_{supply} (mA)
p1	Sleep	Off	Standby	.280
p2	8.0	Off	Standby	1.08
p3	8.0	Standby	Standby	1.14
p4	8.0	9	100	1.83
p5	4.0	9	100	1.49
p6	2.0	9	50	1.05
p7	1.0	9	25	.850
p8	8.0	Off	Rx mode	21.71

Table 1: Sample power modes, V_{DD} = 2.8V, Message = 256 bytes

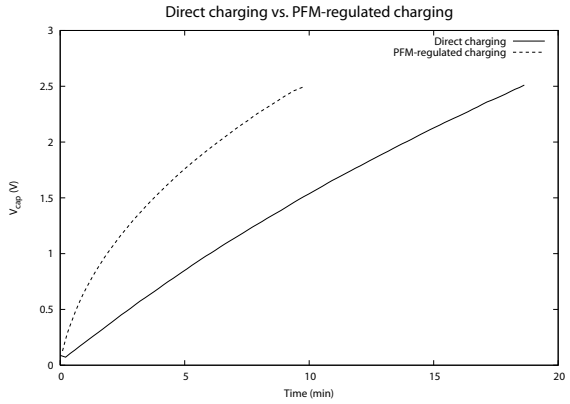

Figure 6: Comparison between direct capacitor charging and PFM-regulated charging

into the packet eliminating the need for error checking.

5. EXPERIMENTAL RESULTS

Three metrics determine the performance of the Everlast board: efficiently charging the supercapacitor, tracking the solar cell at MPP, and running continuously 24 hours a day.

Fig. 6 shows a comparison of charging a 10F supercapacitor from a fixed-intensity halogen light source with direct and PFM-regulated charging modes. With direct charging the solar cell is attached to the capacitor while PFM-regulated charging is done through the Everlast board. The latter charging scheme tracked the optimal power point to generate maximum solar power and charged the supercapacitor in about half the time. This makes more energy available for consumption by the sensor node, or enables the node to use a smaller, cheaper solar cell. With future improvements to the regulator efficiency, the gap between these two schemes should widen even further.

Using a solar profile generated from a DC sweep of the solar cell throughout the day, the voltage and current tracking constants, $K_{V_{mp}}$ and $K_{I_{mp}}$, respectively, are calculated and shown in Fig. 7. Voltage tracking is preferred, because under normal lighting conditions, $K_{V_{mp}}$ is between 0.68∼0.72 and reaches up to 0.80 in low light conditions. This is much better than the wide swing range of the current tracking constant. The V_{oc} can also be easily measured by periodically shutting down the regulator with a timer and then sampling the voltage with an ADC or sample-and-hold circuit. Using this method, Fig. 8 shows that the voltage tracking method, with $K_{V_{mp}}$ fixed at 0.70, can track solar power very closely to the DC sweep (hill-climbing) method but without the need for a MCU/DSP and within a few milliseconds needed to sample the open-circuit solar voltage. The voltage tracking method has a tracking error of

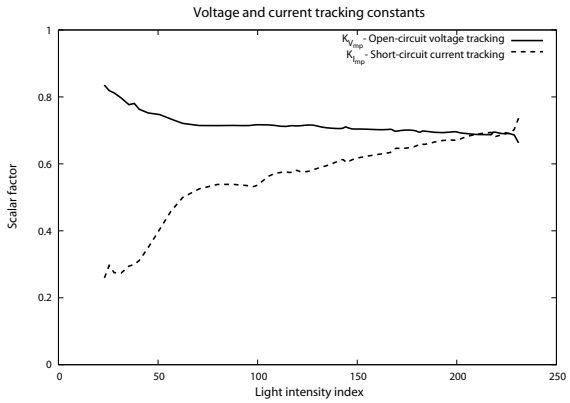

Figure 7: Voltage and current tracking constants calculated over one day

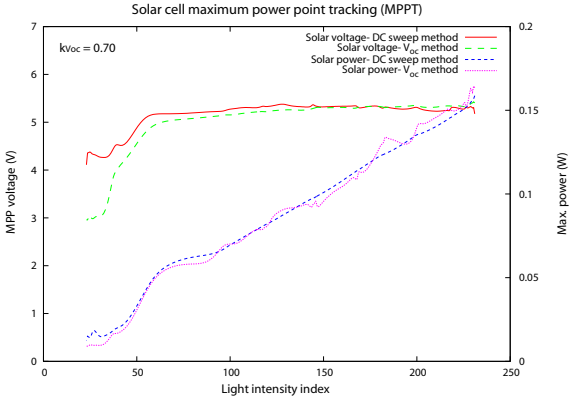

Figure 8: MPPT comparison between DC sweep and V_{oc} method

less than 5% in normal lighting conditions and less than 11% in low lighting conditions in comparison to the DC sweep method. The tracking error increases in low lighting conditions, because the solar cell's $K_{V_{mp}}$ reaches 0.80 while the voltage tracking constant is still fixed at 0.70 in the tracking circuitry. This level of accuracy is acceptable for sub-Watt solar power generation, since the voltage tracking method can be implemented with a few inexpensive, discrete components, and the power requirements to operate a more accurate tracker would outstrip the increase in power generation.

The module must also be able to solely rely on stored energy in the absence of solar power. Creating a few sample modes in Table 1, it is worth noting that the transceiver can continuously transmit 25.6 kbps in profile p5, drawing only 1.49mA. Off a fully-charged 100F supercapacitor, p4 ran for 8.16 hours, p5 ran for 9.54 hours, and p6 ran for 11.1 hours. One point to mention is that the step-up regulator is only 40-50% efficient as it steps up V_{cap} of 1V–2.5V to 2.8V. One area to explore in the future will be to split the power supply rails to the components: 2.0V regulator supplying power to the MCU and transceiver, and 2.7V supplied to any ICs that require it. This will reduce the power consumption of the modules and increase efficiency, which should nearly double the autonomous operating time of each profile.

Fig. 9 is a stress test of Everlast running in p6 on a building rooftop draining the capacitor at night and recharging during the day. In fact, all the data generated in the graph are sampled by the

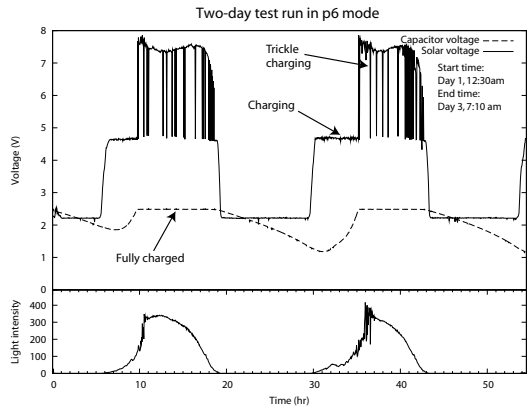

Figure 9: Two-day stress test

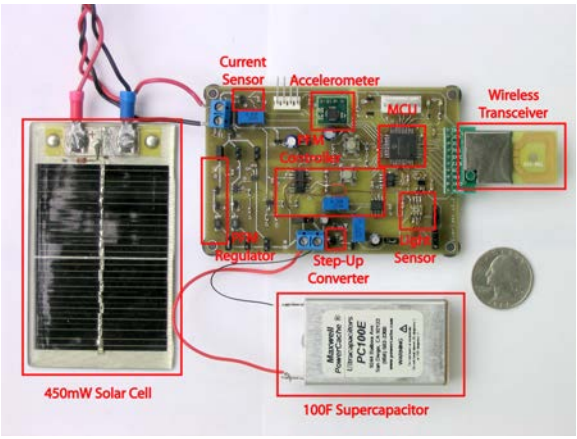

Figure 10: Everlast prototype board

on-board ADC and transmitted from the sensor node itself to a base station. Taking a close look at the graph, throughout the night, the capacitor is drained, and during the morning, the regulator turns on and charges the capacitor. By high noon, the capacitor is fully charged at 2.5V, and the regulator is shut down, causing the solar voltage to jump to V_{oc}. During the day, the sensor node is still transmitting data and drains power from the capacitor. Once V_{cap} dips below 2.45V, the MCU restarts the regulator to recharge the capacitor back to full capacity. After the module is completely charged up, the regulator periodically "trickle charges" the capacitor back to full charge. As solar power decreases in the late afternoon, the power generation is lower than consumption and the capacitor starts to discharge.

6. CONCLUSION

The Everlast sensor node shatters the current preconceptions of designing a sensor node towards only a single goal of either long-life, high data rates, or low cost. With the the replacement of the battery with the supercapacitor, sensor nodes can operate for 20 years while maintaining high data rates. Using a feedforward PFM regulator with open-circuit voltage MPPT, the Everlast system charges the capacitor efficiently by enabling the solar cell to generate maximum power. More accurate MPPT and higher efficiency can be achieved with some fine-tuning of the present design. Future work on the consumption side includes lowering supply rail voltages and exploring multiple capacitor configurations for an expected power reduction by a factor of 2.

Acknowledgments

This work was supported in part by the National Science Foundation grant CCR-0205712 and NSF CAREER Award CNS-0448668.

7. REFERENCES

[1] B. Warneke, M. Last, B. Liebowitz, and K.S.J. Pister. Smart Dust: communicating with a cubic-millimeter computer. *Computer*, 34:44–51, Jan. 2001.

[2] J.M. Rabaey, M.J. Ammer, J.L. da Silva, Jr., D. Patel, and S. Roundy. PicoRadio supports ad hoc ultra-low power wireless networking. *Computer*, 33:42–48, July 2000.

[3] Crossbow Technology. Mica2 datasheet. `www.xbow.com`.

[4] V. Raghunathan, A. Kansal, J. Hsu, J. Friedman, and M. Srivastava. Design considerations for solar energy harvesting wireless embedded systems. In *Proc. 4th Int. Conf. on Information Processing in Sensor Networks*, pages 457–462, Apr. 2005.

[5] P. Enjeti, J.W. Howze, and L. Palma. An approach to improve battery run-time in mobile applications with supercapacitors. In *IEEE 34th Annual Power Electronics Specialists Conference*, 2003.

[6] T.A. Smith, J.P. Mars, and G.A. Turner. Using supercapacitors to improve battery performance. In *Power Electronics Specialists Conference*, 2002.

[7] L. Gao, R.A. Dougal, and S. Liu. Active power sharing in hybrid battery/capacitor power sources. In *Eighteenth Annual IEEE Applied Power Electronics Conference and Exposition*, 2003.

[8] X. Jiang, J. Polastre, and D. Culler. Perpetual environmentally powered sensor networks. In *Proc. 4th Int. Conf. on Information Processing in Sensor Networks*, pages 463–468, Apr. 2005.

[9] Maxwell Technologies. BCAP0350 datasheet. `http://www.maxwell.com`.

[10] H. Pollock. High efficiency, high frequency power supplies for capacitor and battery charging. In *IEE Colloquium on Power Electronics for Demanding Applications*, pages 901 – 910, Apr. 1999.

[11] R.M. Nelms and J.E. Schatz. A capacitor charging power supply utilizing a ward converter. *IEEE Trans. Ind. Electronics*, 39:421–428, Oct. 1992.

[12] K.H. Hussein, I. Muta, T. Hoshino, and M. Osakada. Maximum photovoltaic power tracking: an algorithm for rapidly changing atmospheric conditions. In *IEE Proceeding Generation, Transmission and Distribution*, pages 59–64, Jan. 1995.

[13] C. Hua and C. Shen. Study of maximum power tracking techniques and control of DC/DC converters for photovoltaic power system. In *IEEE-PESC. Conf. Rec.*, pages 86–93, 1998.

[14] E. Koutroulis, K. Kalaitzakis, and N.C. Voulgaris. Development of a microcontroller-based, photovoltaic maximum power point tracking control system. *IEEE Trans. Power Electronics*, 16:46–54, Jan. 2001.

[15] Y. Kuo, T. Liang, and J. Chen. Novel maximum-power-point-tracking controller for photovoltaic energy conversion system. *IEEE Trans. Ind. Electronics*, 48:594–601, June 2001.

[16] T. Noguchi, S. Togashi, and R. Nakamoto. Short-current pulse-based maximum-power-point tracking method for multiple photovoltaic-and-converter module system. *IEEE Trans. Ind. Electronics*, 49:217–223, Feb. 2002.

[17] J.H.R. Enslin, M.S. Wolf, D.B. Snyman, and W. Swiegers. Integrated photovoltaic maximum power point tracking converter. *IEEE Trans. Ind. Electronics*, 44:769–773, Dec. 1997.

[18] Dong-Yun Lee, Hyeong-Ju Noh, Dong-Seok Hyun, and Ick Choy. An improved MPPT converter using current compensation method for small scale pv-applications. In *IEEE 18th Annual Applied Power Electronics Conf. and Expo.*, 2003.

[19] D.L King, J.A. Kratochvil, and W.E. Boyson. Field experience with a new performance characterization procedure for photovoltaic arrays. In *In Proc. 2nd World Conf. and Exhib. on Photovoltaic Solar Energy Conversion*, 1998.